

Exoplanet System *Kepler-2* with comparisons to *Kepler-1* and 13

Michael D. Rhodes¹ • Çağlar Püsküllü² •
Edwin Budding^{2,3,4,5} • Timothy S. Banks⁶

Abstract

We have carried out an intensive study of photometric (Kepler Mission) and spectroscopic data on the system *Kepler-2* (HAT-P-7A) using the dedicated software WINFITTER 6.4. The mean individual data-point error of the normalized flux values for this system is 0.00015, leading to the model’s specification for the mean reference flux to an accuracy of ~ 0.5 ppm. This testifies to the remarkably high accuracy of the binned dataset, derived from over 1.8 million individual observations. Spectroscopic data are reported with the similarly high-accuracy radial velocity amplitude measure of ~ 2 m s⁻¹. The analysis includes discussion of the fitting quality and model adequacy.

Our derived absolute parameters for *Kepler-2* are as follows: M_p (Jupiter) 1.80 ± 0.13 ; R_* $1.46 \pm 0.08 \times 10^6$ km; R_p $1.15 \pm 0.07 \times 10^5$ km. These values imply somewhat larger and less condensed bodies than previously

catalogued, but within reasonable error estimates of such literature parameters.

We find also tidal, reflection and Doppler effect parameters, showing that the optimal model specification differs slightly from a ‘cleaned’ model that reduces the standard deviation of the ~ 3600 binned light curve points to less than 0.9 ppm. We consider these slight differences, making comparisons with the hot-jupiter systems *Kepler-1* (TrES-2) and 13.

We confirm that the star’s rotation axis must be shifted towards the line of sight, though how closely depends on what rotation velocity is adopted for the star. From joint analysis of the spectroscopic and photometric data we find an equatorial rotation speed of 11 ± 3 km s⁻¹.

A slightly brighter region of the photosphere that distorts the transit shape can be interpreted as an indication of the gravity effect at the rotation pole; however we note that the geometry for this does not match the spectroscopic result. We discuss this difference, rejecting the possibility that a real shift in the position of the rotation axis in the few years between the spectroscopic and photometric data-collection times. Alternative explanations are considered, but we conclude that renewed detailed observations are required to help settle these questions.

Keywords Stars – Binary · Exoplanets · Light curve analysis

1 Introduction

Different techniques in exoplanet discovery and research have been selectively applied to, or alternatively have led to the characterization of, different types of object. The *Kepler* Mission has detected a relatively large

Michael D. Rhodes

Brigham Young University, Provo, Utah, USA

Çağlar Püsküllü

Çanakkale Onsekiz Mart University, Çanakkale, Turkey

Edwin Budding

University of Canterbury, Christchurch, New Zealand

Timothy S. Banks

Nielsen, Chicago, USA

¹Brigham Young University, Provo, UT 84602, USA

²Dept. of Physics, Çanakkale Onsekiz Mart University, TR-17020, Çanakkale, Turkey

³Dept. Physics & Astronomy, University of Canterbury, New Zealand.

⁴SCPS, Victoria University of Wellington, P.O. Box 600, Wellington, New Zealand

⁵Carter Observatory, 40 Salamanca Rd, Wellington, New Zealand

⁶Data Science, Nielsen, 200 W Jackson Blvd, Chicago, IL 60606, USA. Email: tim.banks@nielsen.com Tel:+1-847-284-4444

proportion of ‘hot jupiters’, while high-resolution spectroscopy has located many objects of comparable mass but often further from the host star, spectroscopy being less selective in what it can sample. Spectroscopy has, however, proved to have highly significant applications to certain *Kepler* targets — as studied below. Neuhäuser et al. (2011) have reviewed the relevant general background.

Borucki et al. (2003) set out the aims of the original *Kepler* Mission within the context of exoplanet research, while a comprehensive early summary was that of Borucki et al. (2011). The Kepler Science Center manages the interface between the scientific mission and the *Kepler* data-using community. Importantly, data are freely and easily available from the NASA Exoplanet Archive (NEA-website).

Rhodes & Budding (2014) developed and applied the program WINFITTER 6.4¹ to the analysis of *Kepler* exoplanet light curves and found their results to compare favourably with those of other research groups. Occasional small differences in such results, and their significance, were discussed by Budding et al. (2016), including the case of *Kepler-1*. Apparent peculiarities of *Kepler-1* have been previously remarked on (Kipping & Spiegel, 2011) regarding the exoplanet’s low albedo and possible variations of other parameters. Such effects are further discussed below. The fitting program WINKEPLER (Rhodes & Budding, 2014), has been reworked and upgraded to the version WINFITTER 6.4 (cf. Budding et al., 2018), used in the present study. WINFITTER 6.4 includes an option for fitting the radial velocity curve, including the effects of eclipses and proximity, in a parallel way to the photometric data-fitting. This is pursued in Section 3.

Regarding the data, it should be noticed that the NEA operates an initial ‘pre-search data conditioning’ (PDC) process aimed at removing systematic, but non-object-related, trends. The methods applied for this have evolved with growing experience of the system (Twicken et al., 2010; Smith et al., 2012; Stumpe et al., 2012). The resulting PDCSAP fluxes are given in the output columns of the data worksheets released by the NEA. Different opinions have been voiced about this, but the PDCSAP fluxes can be checked by users for their self-consistency within their own programmes. This approach is in regular use by NEA data analysts and is followed in the present study.

This paper discusses optimised fittings of a suitable function to selected NEA-sourced data-sets in terms of parameters that characterize relevant physical effects. We concentrate on the hot-jupiter containing, relatively

well-known, systems *Kepler-1* (TrES-2, discovered by O’Donovan et al., 2006), -2 (HAT-P-7, discovered by Pál et al., 2008) and -13 (Borucki et al., 2011), with a new WINFITTER analysis of *Kepler-2* being the main focus of the present work. We include comparisons of our results with previous analyses of *Kepler-1* and -13.

It should be demonstrated that specified parameters satisfy formal determinacy conditions. At the same time, the adequacy of the WINFITTER model to explain the effects needs to be examined. These issues have been clarified in previous papers on *Kepler* exoplanet light curves (cf. Budding et al., 2018). For this system we used the transit derived parameters from Welsh et al. (2010) and the stellar parameters derived through asteroseismology by Christensen-Dalsgaard et al. (2010).

A significant point concerns increasing confidence in the published properties of exoplanets arising from the cross-comparisons of results from different investigations.

2 Prior information

In Table 1 we summarize the prior information available from the NEA or literature sources (e.g. Batalha et al., 2013)² needed to reach a full set of results from the *Kepler* light curves. In preparing this table we have taken into account parameters listed by various other authors; including the sources listed in our previous studies of *Kepler-1* and -13, (Budding et al., 2016 & 2018; as well as numerous other papers on *Kepler-2*, including Pál et al., 2008; Winn et al., 2009; Narita et al., 2009; Welsh et al., 2010; Christensen-Dalsgaard et al., 2010; Faigler et al., 2013; Lund et al., 2014; Angerhausen et al., 2015; Esteves et al., 2015; Masuda, 2015; and others).

Our Table 1 numbers contain rounded averages from these sources. Note, though, that the main derivables from photometric analysis are not so dependent on absolute parameter specification. Fittings to the transit minima alone lead directly to relatively well-defined estimates for r_1 , k and i (the radius of the star expressed as a fraction of the semi-major axis of the orbit, the ratio of planet to stellar radii, and the orbital inclination).

With regard to representative values for the planets’ mean surface temperatures T_p , we can write (cf. Catling & Kasting, 2017)

$$T_p \approx T_\star (1 - A_B)^{1/4} \sqrt{r_1/2} \quad , \quad (1)$$

²Parameters listed on the NEA website are in a process of intermittent revision and upgrading.

¹The program was called WINKEPLER in 2014.

where T_* is the star’s effective surface temperature and A_B is the Bond albedo (= 0 for a ‘black body’).³

2.1 *Kepler-1*

Kepler-1 (= KOI 1.01; KIC 11446443)⁴ was first designated TrES-2b by the Trans-Atlantic Exoplanet Survey (TrES) (Alonso et al., 2004). This relatively bright system was intended to be within the limited field of view of the original *Kepler* survey. Relevant evaluations of its properties were published before the launch of the *Kepler* spacecraft (O’Donovan et al., 2006; Sozzetti et al., 2007; Winn et al., 2009). Derived mass and radius values indicated a gas giant having a composition and structure similar to Jupiter, but relatively close to its star. It thus became an early representative of the hot jupiter type of exoplanet. The host star GSC 03549-02811 is at an estimated distance of ~ 250 pc (Sozzetti et al., 2007; Rhodes & Budding, 2014).

It was noted relatively early (Daemgen et al, 2009) that TrES-2b is in a visual binary system: a point that needs to be taken account of in the photometric analysis. O’Donovan et al. (2006) and Sozzetti et al. (2007) also took into account spectroscopic data. They derived fairly consistent mass and radius values for the planet of about $1.2 M_{\text{Jup}}$ and $1.2 R_{\text{Jup}}$, respectively. Further details can be found in our previous study (Budding et al., 2016).

2.2 *Kepler-2*

This exoplanet system is also known as HAT-P-7Ab, 2MASS J19285935+4758102, TYC 3547-01402-1b, KIC 10666592 and BD+47 2846b. The ‘b’ suffix on the BD number shows that *Kepler-2* is also in a visual binary system. However, the separation in Kepler’s camera is about 30 pixels; sufficiently distant to prevent significant image contamination from the companion (Dotson, 2013; Libralato et al., 2016). The planet’s 10.5 mag host star has been associated with a late A to mid-F type classification: a Main Sequence object situated at about 350 pc distance. Its ‘hot jupiter’ companion, that produces a $\sim 0.67\%$ variation of light, was also discovered before the launch of the Kepler satellite in 2009 (Pál et al., 2008) and the system has figured in numerous studies and survey articles over the last decade.

Measurements attributed to the Schlesinger-Rossiter-McLaughlin effect⁵ (Schlesinger, 1910; Rossiter, 1924;

McLaughlin, 1924) suggested a high angle ($\gtrsim 90^\circ$) between the stellar equator and the planetary orbit (Winn et al., 2009; Narita et al., 2009; Albrecht et al., 2012). The implied retrograde motion (the first such example, cf. Narita et al., 2009) is awkward to explain directly from the classical ‘nebular hypothesis’ of planet system origins: something additional is sought. Planet-planet scattering, or a Kozai effect, may be involved though only one planet has been definitely identified in the system so far.

Welsh et al. (2010) announced their discovery of tidal effects in the light curve, the first exoplanet light curve to be so characterized. Borucki et al. (2009) reported the light curve to be consistent with a strongly absorbing atmosphere above the planet, but with limited heat transport to the night side. On the other hand, Esteves et al. (2015) drew attention to changes of phase of the system’s peak brightness, possibly arising from inhomogeneous clouds and/or substantial atmospheric winds. They related these to albedo values and the planet’s overall energy budget, although the system was not included with the ‘super-rotation’ candidates listed by Angerhausen et al. (2015).

Alternative ideas on brightness anomalies were initiated by Morris et al. (2013), who considered a spot-like gravity darkening effect. Van Eylen et al. (2013), studying a larger data sample, cautioned about the possibility of instrumental artefacts, a noteworthy point in the context of *Kepler-2*’s known visual companion (see also, Lund et al., 2014). Masuda (2015) applied gravity-effect analysis to the complete data-set, finding general support for a near-pole-on configuration.

Masuda (2015) also referred to the previous work of Benomar et al. (2014) and Lund et al. (2014) on *Kepler-2*, that included detailed discussions of the results of asteroseismology. Due to the very low noise levels and uninterrupted long-term data monitoring with short sampling cadences, satellite-based photometry may allow asteroseismological techniques to recover basic stellar parameters with relatively high precision. Further background on such applications can be found in the collection of papers from Shibahashi & Lynas-Gray (2013), Guzik et al. (2014) and others. Even greater information yield, or confidence on parameter estimates, can be gained when such information is combined with other forms of data, or approaches to analysis (e.g., Lillo-Box et al, 2016).

Benomar et al. (2014) noted that the apparent profiles of rotationally induced frequency multiplets are sensitive to the angle between the line of sight and the star’s rotation axis (usually denoted i_*), permitting a good estimate of its value from asteroseismology. However, differences exist between parameters from differ-

³The Earth’s mean surface temperature, estimated in this way, is ~ 280 K, while the regular GISS measure is close to 287 K.

⁴KIC stands for Kepler Input Catalogue, KOI for Kepler Object of Interest.

⁵Often just referred to as the Rossiter effect.

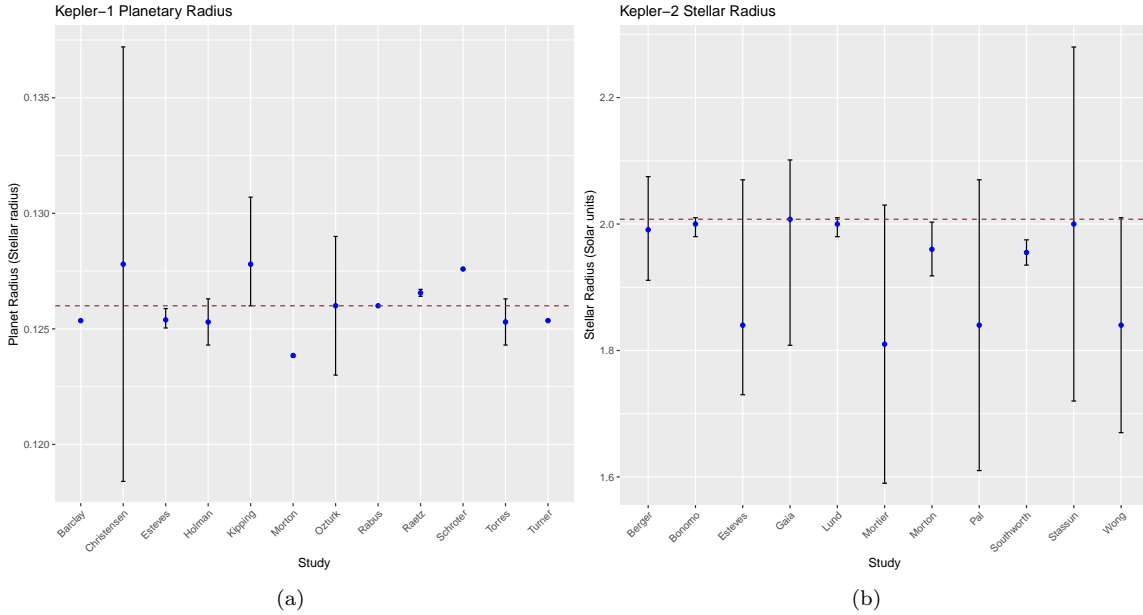


Fig. 1 Example Comparison of starting information: sub-figure(a) shows the planetary radii taken from the NEA summary page for Kepler-1, and sub-figure (b) plots the stellar radii for Kepler-2. The initial starting estimates used by the current study are shown as brown dotted lines. Papers are referred to by their lead author, with reference details available on the appropriate NEA summary webpage. The Gaia DR2 (Gaia Collaboration, 2018) is referred to as ‘Gaia’. Where Gaia data were available we used these in preference to our mean values (as in sub-figure (b)). These representative charts are to show that our starting estimates are in line with the literature, and also to demonstrate the wide spread in error estimates across studies (which were taken as reported by the individual studies).

Table 1 Primary Input Data

KOI	L_1	M_*	R_*	T_*	T_p	λ	Epoch	P
1.01	0.9683	1.06	0.98	5850	1350	6220	2454849.52664	2.47061892
2.01	1.000	1.56	2.01	6390	2000	6140	2454954.358470	2.204740
13.01	0.55	2.27	2.70	8500	2500	5970	2455138.7439	1.7635877

The notation here is: L_1 – fractional luminosity of host star taking into account the companion (see Section 2.1), M_* – mass of star (solar masses), R_* – radius of star (solar radii), T_* – temperature of star (K), λ – effective wavelength (Å), P – orbital period (in days). The numbers given in this table are rounded averages from results in the cited literature and sources provided by the NEA (see text and also Figure 1), bar where Gaia DR2 figures were available and therefore adopted.

ent investigations using these techniques. For example, according to Benomar et al. (2014) the host-star’s mass (M_* in solar units for this and the following) is 1.59 ± 0.03 ; Lund et al. (2014) have it at 1.51 ± 0.04 or 1.63 ± 0.09 , using different models; van Eylen et al. (2013) find 1.36 ± 0.02 ; while Christensen-Dalsgaard et al. (2012) report 1.52 ± 0.04 . The latter is close to the average value of these estimates, though the standard deviation is about 7% of that mass.

More recently, Wong et al. (2016) examined infrared data on *Kepler-2* from the Spitzer Space Telescope. Their measured depths of the secondary eclipses were consistent with a relatively high daytime representative temperature of ~ 2650 . With the aid of detailed atmospheric modelling, their analysis pointed to a relatively

inefficient day-night heat circulation for *Kepler-2*. An eastwardly shifted ‘hotspot’, which has been associated with a super-rotating equatorial jet in comparable studies of this and other hot jupiters (Faigler et al., 2013; Faigler & Mazeh, 2015), was not detected by Wong et al. (2016), though the models they used were not consistent with all aspects of the data.

On the other hand, Armstrong et al (2016) repeated earlier findings of shifts of peak brightness, and suggested recurrent movements of a hot spot from one side the of the planet’s substellar point to the other on timescales of tens to hundreds of days. Their interpretation involved significant variations in global wind patterns and related cloud coverage.

Table 1 Primary Input Data (contd.)

KOI	$\bar{\rho}_*$	$\bar{\rho}_p$	Z	$\log g$	a	M_p/M_*	R_p/R_*	u_1	A_g
1.01	1.44	0.90	-0.15	4.44	0.0353	0.0013	0.1260	0.64	0.03
2.01	0.27	0.61	-0.15	4.07	0.03676	0.0012	0.081	0.48	0.27
13.01	0.16	1.00	-0.141	3.94	0.0349	0.0036	0.0855	0.44	0.61

The notation is now: $\bar{\rho}_*$ – star’s mean density (CGS), $\bar{\rho}_p$ – planet’s mean density, Z – metallicity of star, $\log g$ – \log_{10} of the surface gravity of star (cgs units), a – semi-major axis in AUs, M_p/M_* – ratio of planet to star masses, u_1 – stellar (linear) limb-darkening coefficient. The numbers given in this table are rounded averages from results in the cited literature and sources provided by the NEA (see text).

The distribution of individual observations, for example in Fig 2 of Armstrong et al. (2016), shows that the proportion of points whose error bars are completely missed by the fitted model curves is much greater than might be expected. In other words, systematic short-term effects are present in the data that are unaccounted for by generic models for the complete phase-range. Precipitation of crystallised alumina has been proposed to explain the clouding in the hot conditions experienced by this exoplanet, leading to a picturesque description of “raining rubies and sapphires” in popular reports (see Armstrong *et al.*, 2016, for the source paper and Dvorsky (2016) for an example of a popular report).

Given the possibility of over-detailed modelling, leading to parameter indeterminacy, a relatively simple summary of clouding effects was proposed by von Paris et al. (2016) on the basis that they would cause asymmetric primary transits due to a predominance of cloud towards the western (‘morning’) limb of the planet (the leading limb in primary transit). The eastern limb, which becomes visible as the planet recedes after mid-transit, is relatively cloud-free in this scenario. There has been a common assumption of super-rotating winds above a rotationally synchronized planet body in cloud-formation discussions. Clouds formed to a greater extent on the unilluminated hemisphere are then transported to the morning sector that would become more visible on approach. In view of an expected high opacity at the cloud tops, the planet could have different apparent radii for the two sides of the eclipse.

Still, ambiguity remains about the possible causes of minimum asymmetry and light curve anomalies.

2.3 *Kepler*-13

The near-10th magnitude exoplanet-containing system *Kepler*-13 was identified early in the mission’s output (Borucki et al., 2011) and given the designation KIC 9941662 (Brown et al., 2011) after the first two quarters of data collection (see also Rowe et al., 2011). This complex, massive hot jupiter has an orbital period of

~ 1.764 d and an (asymmetric) transit depth of about 0.45% of full light. Numerous papers have been presented on the system, as briefly summarized in our previous contribution (Budding et al., 2018).

Rhodes & Budding (2014) remarked on KOI-13.01 as of special interest from even early studies, since proximity effects and a secondary minimum are noticeable even from preliminary inspection. These are not commonly observed features of exoplanet light-curves (Esteves et al., 2013). Rhodes & Budding essentially confirmed the mass ratio of Mislis & Hodgkin (2012), while their value for the planet’s mass ($9.4 \pm 1.4 M_J$) was somewhat closer to the estimate of Mazeh et al. (2012).

Barnes et al. (2011) first called attention to the fact that photometry of *Kepler*-13 may be compromised by the relatively bright companion star, entailing slight shifts of the light centre on the detection array affecting the data. Basically, the aperture was set too small for the first two quarters of data-acquisition, and so data from those quarters have been subsequently disregarded. Having then restricted their attention to the later short-cadence photometry, Barnes et al. (2011) interpreted apparent variations in the detailed shape of the light curve minima as arising from a gravity-darkened, rapidly rotating, host star, scanned by the planet’s transit with particular spin-orbit configurations relative to the line of sight.

Numerical details in the model of Barnes et al. (2011) were challenged by Johnson et al. (2014) who used a spectrographic, Doppler-tomographic technique that indicated KOI-13.01 has a different orbit orientation to that given by Barnes et al. (2011). But interdependence of modelling parameters in this kind of data-analysis should be kept in mind. The planetary path followed in the model of Barnes et al. (2011) may need to pass closer to the pole, increasing the relevant tilt-angle (λ), if that pole were not as bright. Hence, the relative scale of an adjustable gravity-darkening could be weaker and the model of Barnes et al. still hold, but with a different angle of tilt.

Mislis & Hodgkin (2012) confirmed that the planet orbits the slightly brighter of the two stars (cf. Santerne

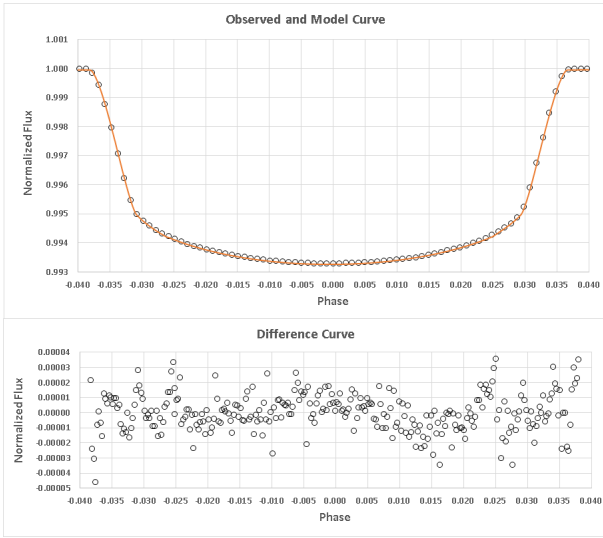


Fig. 2 The transit region for *Kepler-2b*, matched by a basic WINFITTER model. The fitting-function will allow shifts of the rotation axis position and rotation rate, and a quadratic limb-darkening prescription, but these are not used in the initial fitting. The corresponding residuals are shown in the lower panel. A systematic drop of about 0.00002 of the mean flux level, centred on phase ~ 0.015 can be noticed. This could be interpreted as the planet passing over a brightened region of surface: feasibly a gravity-brightened polar region of the star.

et al., 2012) and also confirmed that it has its own small, but detectable, light flux in the broad, near-IR-containing, Kepler passband.

3 New study of Kepler-2

We continue along the lines of our previous papers on *Kepler-1* and -13 in dealing with the data on *Kepler-2*.

3.1 Preliminary photometric analysis

We used the program WINFITTER 6.4 (Rhodes, 2019) to analyse the available normalized PDCSAP short cadence data sets covering the observing quarters 0-17, downloaded from the NASA Exoplanet Archive. The given times of observation (BKJD) were converted to phases in the range 0.0 to 1.0, using the ephemeris given in Table 1. This produced a total of 1,879,376 individual observations for the initial data-set. WINFITTER has a binning application, which was used to bin the data-set with a 500 to 1 ratio down to 3758 individual points. This enabled a faster exploration of data-space, with negligible loss of mean parameter validity. An error measure is published with each flux measurement on the NEA data-source. We assume Poissonian statistics and infer a binned error measure by dividing the

original by \sqrt{N} where N is the number of points in the bin. From this complete light curve, we extracted 374 data points covering the phase region -0.05 to $+0.05$ to enable detailed analysis of the transit.

The downloaded PDCSAP fluxes have been preliminarily normalized to unity, but the process of optimizing the model-fitting allows for slight variations of this quantity. For exoplanet light curves, we set, at least initially, the reference light level $U = L_1$ (fractional light of eclipsed star). The transit region has a relatively large information content per datum for the main geometric and limb-darkening parameters (r_1 , k , i , and u_1). Having found good estimates for these parameters, the more slowly varying, low-amplitude out-of-eclipse flux changes can be used more effectively to bear on other parameters — such as the mass ratio, gravity-effect, or reflection coefficients (q , τ , E).

Background to the program WINFITTER⁶ was presented in some detail by Budding et al. (2018). The current version is WINFITTER 6.4. It continues to be checked and upgraded when necessary. WINFITTER uses a modified Marquardt-Levenberg technique to perform its optimization procedure. Its fitting function is based on the *Radau* model developed from Kopal’s (1959) presentation of the tidal and rotational distortions (‘ellipticity’), and an appropriate description of the radiative interactions (‘reflection’). The photometric Doppler effect (Hills & Dale 1974; Shporer et al., 2012) is also included in the calculations. The algebraic form of the fitting function allows large regions of the χ^2 -parameter hyperspace to be explored at low computing cost.

Optimal models produced by WINFITTER correspond to the least value of χ^2 , defined as $\Sigma(l_{o,i} - l_{c,i})^2 / \Delta l_i^2$ (Bevington, 1969), where $l_{o,i}$ and $l_{c,i}$ are observed and calculated light levels at a particular phase. Δl_i is an error estimate for the measured values of $l_{o,i}$. The NASA Exoplanet Archive (NEA) lists empirical values of Δl_i for each datum, whose mean allows a suitable setting for the mean datum error Δl in WINFITTER. The χ^2 Hessian is numerically evaluated in the vicinity of the χ^2 minimum. Inspecting this matrix, in particular its eigenvalues and eigenvectors, gives insight into parameter determinacy and interdependence. The Hessian is inverted to yield the error matrix. This must be positive definite if a determinate optimal solution is to be evaluated. Application of this provision entails that over-fitting of the data is avoided.

For further information on WINFITTER and related issues see Budding et al. (2018). Relevant early papers are Budding (1974) and Banks & Budding (1990).

⁶The latest version of WINFITTER is downloadable from <http://michaelrhodesbyu.weebly.com/astronomy.html>

The results of the initial transit analysis are summarized in Fig 2 and Table 2. Adopted bolometric gravity-darkening and luminous efficiency coefficients are listed in this table. These are converted to the values applying at particular wavelength and effective temperature combinations using the black body approximations specified by formulae 9.18 and 9.19 in Budding & Demircan (2007) using relevant data from Table 1. These coefficients have relatively little effect for the primary transit region of the light curve, though they will be required in subsequent analysis. In practice, at least in the first approximation to exoplanet light curves, it is only the star’s gravity effect τ_1 and the planet’s reflection coefficient E_2 that are significant.

The shift from the nominal zero point to recover optimal phasing $\Delta\phi_0$ in Table 2 has the rather large value of 0.233° or 0.00065 in phase. This can be essentially attributed to our use of an earlier NEA epoch of BKJD 121.3578, rather than the revised value in Table 1. That is equivalent to BKJD 121.35847, which will give slightly later phases than those originally adopted. The period estimate has been maintained throughout the 4 year data interval.

In Table 2 it is seen that two linear limb-darkening coefficients have been used. A law which is linear in the cosine of the angle of foreshortening appears adequate for the range of annular phases of the transit (u_1 [a]). At the extreme limb, corresponding to partial eclipses, however, it is well-known that the darkening becomes complex and the simple linear law inadequate for precise modelling of the radiation transfer (Kourganoff, 1952). There will, however, be some representative linear coefficient that can optimally reduce the residuals in the short phase range towards the limb (u_1 [p]), and though the residuals’ scatter can be seen to increase around the partial phases in Fig 2 it is not changed drastically. The device of using a second mean linear coefficient to cover the short range of partial phases is regarded as an artifice, brought about by the complexity of the limb-darkening effect at the extreme limb. This rather coarse approximation is reflected in the somewhat greater variation of residuals through the partial phases, but the net effect on the other fitting parameters is small, while details of the flux emanating from the extreme limb region are not relevant to the main targets of our study.

The adopted single point error is down on the raw datum error (0.00015; Budding and Rhodes, 2014) by a factor of 13.6, but this should be $\sqrt{500} = 22.4$, if the scatter was due only to Poissonian counting noise. It was mentioned already (Section 2.2) that additional sources of deviation, perhaps related to chaotically variable cloud cover, affect the data for *Kepler-2*. However,

Table 2 Initial curve fitting results for the complete set of *Kepler* photometry, binned by a factor of 500, for the transit of *Kepler-2b*. Parameters have their conventional designations as U : the ‘unit of light’; $\Delta\phi_0$: shift of zero point of the phase scale; r_1 : radius of host star in units of the separation of the two mass centres; k : ratio of the radii; i : orbital inclination; u_1 coefficient of the linear term in the limb-darkening law – see Section (3.1). χ^2/ν : reduced χ^2 -value; Δl : adopted mean error of a single datum. The error estimates, applying to adjustable parameters, are derived from the formal error matrix calculated at the adopted optimum. Other fitting-function parameters are discussed in later sections of the paper.

Parameter	Value	Error
U	0.999992	0.000002
$\Delta\phi_0$ (deg)	0.233	0.021
r_1	0.242	0.0004
k	0.0781	0.0001
i (deg)	83.08	0.01
u_1 [a]	0.457	0.002
u_1 [p]	0.481	0.008
τ	1	—
E	1	—
χ^2/ν	0.98	
Δl	0.000011	

Table 2 reflects only a preliminary fitting, and there may remain other systematic effects in the data that WINFITTER’s full modelling parameter set can account for.

Thus, the residuals plotted in Fig 2 show a small, but systematic, depression centred around phase 0.015, that could be associated with the eclipse of a brighter than average region of surface. If this were a polar region, brightened by the gravity-darkening effect, it should inform about the rotational geometry, as in the case of *Kepler-13*. Information on the rotation also derives from the the spectroscopy of *Kepler-2* that we examine next.

3.2 Radial velocity curve

Kepler-2 has been observed with the High Resolution Spectrograph (HIRES) on the Keck I 10 m telescope, as well as the High Dispersion Spectrograph (HDS) on the Subaru 8 m telescope, both instruments at the high altitude Mauna Kea location. Initially, 8 HIRES spectra were gathered by Pál et al. (2008). A further 9 were added by Winn et al. (2009). All but one of these HIRES spectra were from the out-of-eclipse phase range. Some 49 HDS spectra were obtained in June and July, 2009 including a thorough covering of the planetary transit.

Observational details were reported by the foregoing authors, as well as Narita et al. (2009). Essentially, the methods followed to obtain radial velocities (RVs) were the same as those of the California Planet Search (Howard et al., 2009). It may be noted, however, that Pál et al. (2008) refer to Butler et al. (1996) as the basis of their reductional procedure, while Winn et al. (2009) cite Butler et al. (2006) “with subsequent improvements”. The latter reference mentions having introduced considerable revisions to methodology after their earlier work, including a more accurate barycentric correction, as well as changes to hardware that restricted previous precision. Moreover, exoplanet RVs were originally arranged so that the zero point was set to a median value of the RV measures. In the later reference, however, an offset has been fixed after an orbital solution for the system’s mean radial velocity V_γ . Butler et al. (2006) indicate that differences may arise in the reference velocity for the exoplanet RV curve due to these procedural changes, as well as from the binning of groups of individual measurements. These points are relevant, because Winn et al. (2009) comment on a systematic difference in the reference velocity (V_γ in Table 3) between their RV curve and that of Pál et al. (2008), that we look into below.

We adopted the 86 RV values listed by Winn et al. (2009) as the basis of an optimal model fitting using the equivalent (‘Radau’) model used for our photometric analysis but tailored to RV measures. The model accounts for the Doppler effects arising from a Keplerian orbit, but having the spectral line positions corresponding to a centre of light modified by the regular proximity effects that operate in close binary systems (cf. Kopal, 1959, Ch. 5). An eccentric orbit was trialed in the RV-curve fitting, but eccentricity parameters could not be resolved from zero (i.e. a circular orbit) with sufficient confidence from the limited phase coverage.

Table 3 presents the results of fitting a rotating star model to the spectral line shifts, with the assumption that the stellar rotation is typical for Main Sequence stars of this mid-F type. For such a star an equatorial rotation velocity of 30 km s^{-1} could be reasonable (McNally, 1965). Synchronised rotation of the star to the orbital motion would give the relatively high speed of $\sim 46 \text{ km s}^{-1}$ at the star’s equator, hence its rotation parameter γ_1^7 is here set to 0.65.

The corresponding data and model curve are displayed in Fig 3. An inherent ambiguity arises, in that the RV measures only refer to motion in the line of sight.

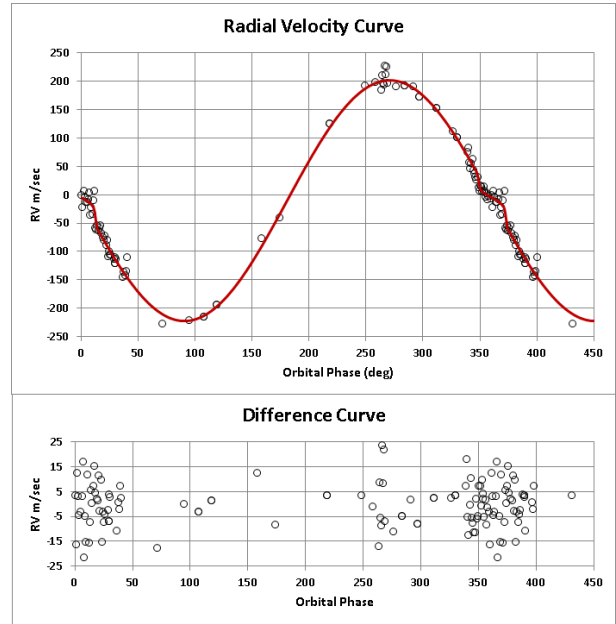


Fig. 3 Optimal fitting to the RV curve of Kepler 2A, using the full data-set cited by Winn et al. (2009). The curve includes an optimized Rossiter effect modelling (Section 3.3), but the sign an amplitude of this is atypical for binary system orbits.

We have located the vector corresponding to a positive rotation when viewed from above, i.e. the ‘north pole’, this being in the third quadrant of the stellar disk as observed at transit. But the same line of sight effect can be produced by putting the negative rotation pole (‘south’) mirrored in the first quadrant, with the planet moving in the opposite direction.

Note that the polar axis points quite close to the line of sight in this fitting (cf. Winn et al., 2009), but this is dependent on the assumed scale of the angular velocities of rotation and revolution, as a consequence of the Rossiter effect. This was mentioned above and is further discussed in the next subsection. If the star’s rotation rate parameter γ_1 is reduced from its adopted value, the pole can move further from the line of sight into the third quadrant of the Earth-facing disk (see Section 3.3).

For the most part, the out-of-eclipse RVs follow the near-sinusoidal trend expected of the star’s slight response to the orbital pull of the planet. However, Winn et al. (2009) noted that there was a systematic shift between the two sets of data gathered in mid-2007 and mid-2009 of some $22 \text{ m s}^{-1} \text{ y}^{-1}$. We checked and used this correction in modelling the combined data-sets.

During the transit phase range we encounter the Rossiter effect, which permits a more detailed characterization of the system’s properties. But in the present case, the effect appears slight and lower than could be

⁷The ratio of the i -th component’s angular velocity of rotation to that of orbital revolution is denoted γ_i in Kopal’s (1959) book (Eqn 5-11 in Ch. 2), though in Budding et al. (2018) it was identified as $\sqrt{\kappa}$.

Table 3 Curve fitting results for the RV measures of Kepler 2A. Parameters have their conventional designations as in Table 1 but now with the addition of K_1 : amplitude of primary’s radial velocity variation; V_γ : mean radial velocity of the star relative to the adopted reference frame (see text); γ_1 : ratio of star’s angular velocities of rotation to orbital revolution; λ : projected angle of tilt of the rotation axis; Δv : adopted mean error of a single datum. The error estimates are derived from the formal error matrix calculated at the adopted optimum. Other parameters are passed from Table 2. The determined velocities are in m s^{-1} .

Parameter	Value	Error
K_1	212.6	2.1
$\Delta\phi_0$	-0.5	0.3
V_γ	-8.6	1.4
i	83.1	
r_1	0.242	
r_2	0.020	
q	0.0011	
$u1$	0.46	
L_1	1.0	
L_2	0.0	
γ_1	0.65	
ϵ	93.8	1.3
ψ	-1.2	1.2
λ	188.8	1.2
χ^2/ν	1.05	
Δv	10.4	

generally expected. In fact, the departures from one continuous sine curve for the complete data-set, given the accepted observational errors of a few m s^{-1} , are sufficiently small as to allow questioning the significance of *any* eclipse effect on the RV measurements (see Fig 3).

We will return to this point: for now, we remark that given the prior mass of the star M_\star from Table 1, the mass ratio q can be determined from a recursive solution of the implicit equation

$$q = f^{1/3}(1+q)^{2/3} , \quad (2)$$

where the mass-function f is given by

$$f = C(1 - e^2)^{3/2} K_1^3 P / (M_\star \sin^3 i) . \quad (3)$$

The values of period P and inclination i needed to solve Eqn(3) are given in Table 1. The velocity amplitude K_1 can be read from the results of the optimal parametrization the RV curve given in Table 3, with the eccentricity e being negligible. A recent value of the constant C is 1.03615×10^{-7} (with M_\star in solar units, P in d and K_1 in km s^{-1}) to a sufficient accuracy (Budding, 2018), which leads to $q = 0.00113$.

As mentioned above, Winn et al (2009) suggested that this could produce a light travel time effect in a bound system with a long enough period. The shift in question implies a drift from regular repetition in the times of minima of order $3 \times 10^8/c$ s (where c is the velocity of light), i.e., seconds only. The period of the system in Table 1 is given to this order of accuracy, or slightly better, (i.e. 6 significant digits after the decimal point for the period in d). It therefore seems feasible to test if any such drift could be detected in the run of $\Delta\phi_0$ values in a quarter-by quarter analysis of the 17 relevant binned light curves.

Results of checking around this point are shown in Figs 4 and 5. While long-term trends in the fiducial parameters $\Delta\phi_0$ and U seem vaguely possible, they can hardly be regarded as significant. Thus, a net advance of ~ 2 s, i.e. a slight tendency for the phase of mid-minimum to *decrease* below zero, in the time of mid-transit over the 17 quarters could be indicated in Fig 5. Winn et al.’s (2009) finding was, however, that the later radial velocities appeared to be affected by an *increase* in the γ -velocity of the system, i.e. a recession behind a regular sequence, though the corresponding data-sets here are separated by a few years.

At the same time, the suggestion of a trend in Fig 5, not greater than the scatter of individual results, but implying a variation in the mean flux from the star of $\sim 10^{-5}$ over the ~ 4 y period of the Kepler mission is not backed by any decisive alternative evidence. So, while there could be some slight indication of γ -velocity variation in the observed times of mid-transit, or other, intermediate-term photometric variations, no systematic effects of this kind can be confidently confirmed from the available data.

Nevertheless, the rather large scale of random variations in these fiducial parameters may have a connection with the discussion of Armstrong et al. (2016), referred to in Section 2.2. We will return to this in Section 4.

3.3 The Rossiter effect

The main points concerning the effect of eclipses of a rotating star on the measured position of its spectral lines can be summarized (to first order) by allowing the simplifying assumption that the rotating star is spherical with radius R_1 , say, which is significantly larger (by $1/k$) than that of the planet where k is a small quantity. We suppose that a spectral line is subject only to a rotational broadening and not concern ourselves directly with limb-darkening, whose effect can be separated from that of source motion in the given situation. We then consider the rotation geometry in relation to a

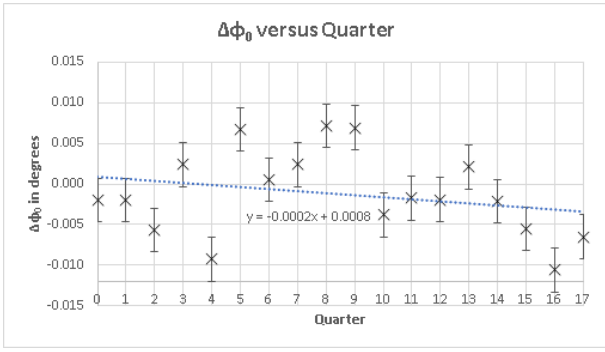


Fig. 4 Trend of correction to predicted mid-transit phases (the parameter $\Delta\phi_0$) over the 17 quarters of the complete data-set for Kepler 2.

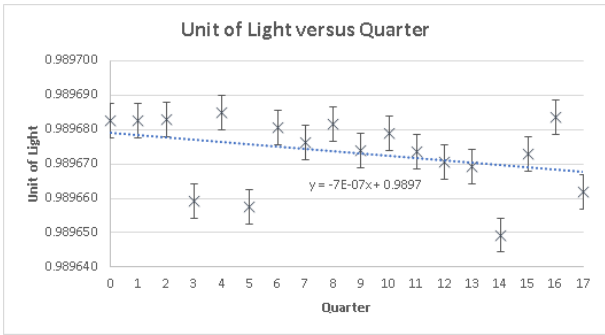


Fig. 5 Trend of reference light levels (the parameter U) over the 17 quarters of the complete data-set for Kepler 2.

conventional (right) x, y, z coordinate system with the z -axis as the line of sight and the planet moving across the stellar disk in the direction of positive x .

On this basis, the effect of the eclipse of the star, rotating with an oblique angular velocity vector $\boldsymbol{\omega}$, may be interpreted as the sum of the effects of the three components of $\boldsymbol{\omega}$: ω_x , ω_y and ω_z . The first of these produces a constant negative or positive net shift (depending on the sign of the impact factor, with ordinate $y = b = \cos i/r_1$); the second a shift that varies linearly from negative to positive or *vice versa* for a retrograde rotation, with central zero; and the third with no RV shift, but a diminution of the effects of the other two components. In combination, these effects constitute the basic ‘Rossiter effect’ of spectral line shifts during the eclipses of rotating stars by exoplanets.

A way to interpret a small amplitude Rossiter effect shown in Fig 6, then, provided the measured shifts correspond to the movement of the line centres in the way presented above (cf. Hirano et al., 2011; Boué et al., 2013; Brown et al., 2017) is that there is a relatively large z component in $\boldsymbol{\omega}$. Unless we have some way to estimate independently the rotation rate for the star, however, the projection angle between z and $\boldsymbol{\omega}$ will have a strong anti-correlation with that rate.

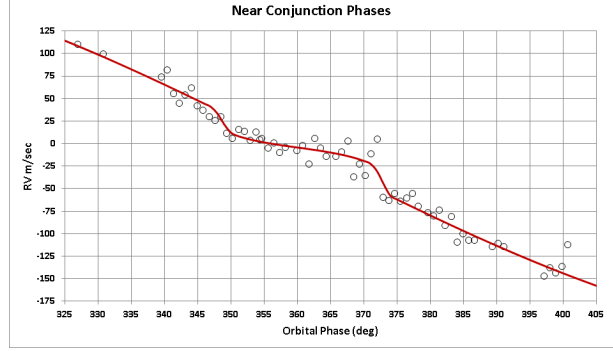


Fig. 6 Close-up of the near-conjunction phases of the RV curve of Kepler 2A using the data-set of (2015). The eclipse effects on the apparent radial velocities can be seen as: (1) relatively low in scale (compared with a feasible amplitude of 10s of m s^{-1}), suggesting a fairly high proportion of ω_z in $\boldsymbol{\omega}$; (2) inverted, with respect to a positively rotating star, suggesting a retrograde rotation, i.e. ω_y points in the opposite direction to \boldsymbol{j} ; (3) although there is significant scatter, the later upward swing above the orbital trend of the excursion, appears greater, in amplitude and extent, than the initial downward swing, suggesting the planet passes over a negative RV associated with ω_x . The net result is that the conventional ‘north’ rotation pole is in the third quadrant in the observer’s xy -plane, not far from the disk centre.

On the other hand, the scale of the net Rossiter shift at the origin, compared with its amplitude, relates to the ratio ω_x/ω_y . This appears directly discernible in Fig 6, and it corresponds to the determinability of the ‘tilt angle’ $\lambda = \arctan(\omega_x/\omega_y)$.⁸ In principle, two angles are involved in locating the position of the rotation pole from that of the orbit: in practice, the angle λ can be estimated directly, whereas the angles ϵ (obliquity) and ψ (precession angle)⁹ tend to show inter-correlation effects to allow constancy of the amplitude/shift ratio in Fig 6. But, given the special condition following from the implied closeness of the line of sight to the disk centre, the angles ϵ and ψ are rather tightly constrained to be close to 90° (ϵ) or small (ψ). And in that case, the formal derivation of λ from i , ϵ and ψ becomes very sensitive to those angle values. Although this special situation cannot be ruled out from the analysis thus far, the greater range of parameter space afforded by

⁸This defines λ as a ‘position angle’, measured clockwise from the y -axis. The value of λ measured in this way was found to be about $205^\circ \pm 10^\circ$. This is compatible with the angle evaluated by Narita et al. (2009), but their number is $\sim 360^\circ$ less than ours. It does not agree with the value adopted by Masuda (2015), who gave an angle less than 180° , which would place the pole in the fourth quadrant of the disk at phase zero, unless perhaps an alternative convention has been followed about the sense of the tilt angle.

⁹In some treatments ψ is used for the obliquity angle. We have followed an older notation in using ϵ (cf. e.g. Allen, 1974).

Table 4 Results of a follow-up set of transit model fittings to the complete (binned) PDCSAP data-set of Kepler 2. Note that the displacement of the rotation axis here does not agree with that in Table 3. This is discussed in Section 4. A quadratic formula for the limb-darkening was adopted. Due to the strong correlation between u_1 and u_2 in this formulation the value of u_1 is significantly larger than its value in Table 2.

Parameter	Value	Error
U	0.998606	0.000003
$\Delta\phi_0$ (deg)	0.007	0.008
r_1	0.2549	0.0001
r_2	0.0202	0.0001
i (deg)	81.10	0.09
u_1	0.553	0.005
u_2	-0.092	—
ϵ (deg)	110.0	—
ψ (deg)	16.6	0.1
γ_1	0.245	0.06
Δl	0.000009	—
χ^2/ν	1.006	—

a significantly lower stellar rotation rate would tend to push the modelling towards that more typical geometrical arrangement.

In fact, Lund et al. (2014) argue for a lower value for the rotation speed, which on the basis of their asteroseismological evidence turns out to be close to 7.66 km sec^{-1} at the equator, implying $\gamma_1 = 0.167$. The average value of $v_{\text{rot}} \sin i_*$ from the 6 independent studies listed by Lund et al. (2014) is $3.35 \pm 1.11 \text{ km sec}^{-1}$. This would allow i_* to deviate by as much as $\sim 25^\circ$ from the line of sight, giving a greater general probability. Lund et al. (2014) cite the comprehensive study of Nielsen et al. (2013) for a comparison of measured stellar rotation periods which, though showing an appreciable scatter, for their adopted F6 type dwarf classification of *Kepler-2* (Feidi et al., 2013) lowers the value of γ_1 from that in Table 3 by a factor ~ 2 . Even so this would still be twice as fast as Lund et al.’s (2014) rotation rate, while the value considered by Masuda (2015), in order to produce the scale of gravity-effect in his modelling of the light curve, required the fast $\gamma_1 \approx 0.94$.

3.4 Further transit analysis

The preliminary photometric model characterized by Fig 2 and Table 2 can be improved by allowing for a non-aligned asynchronous rotation that can account for light curve asymmetry, together with a more refined limb-darkening prescription, as with Kepler 13 (Budding et al, 2018). This entails adjustment of relevant parameters in the light-curve modelling, though,

as with the RV analysis, geometrical ambiguity may arise.

With regard to the depression in Fig 2 (lower panel), if this may be associated with the passage of a planet over a region of surface locally brightened by a rotationally induced polar flattening, the pole being not far from the planet’s path projected onto the surface, then we could expect a light variation of order $r_1^3 \gamma_1^2 k^2 \Phi / 3$ (Budding et al. 2018), where $\Phi < 1$ is associated with the projection geometry. In the present case, this implies the maximum scale of a rotation related anomaly in the transit of *Kepler-2* is about 0.00003, with $\gamma_1 = 1$. Note that bringing the pole closer to the line of sight *enhances* the effect, unlike the situation for the Rossiter effect which is *reduced* by bringing the polar axis closer to the line of sight. This suggests combining photometric and spectroscopic evidence could separate the geometry from the scale of the rotation speed. Unfortunately, the data does not appear to allow a self-consistent picture on this, as we see below.

Given the possibility of the lower obliquity proposed by Lund et al. (2014), the rotation geometry was set with $\epsilon = 110^\circ$ and the curve-fitting allowed for some adjustment of γ_1 . The optimization sequence was aimed at removing the small depression at phase ~ 0.015 , on the assumption that it was a gravity effect. This is essentially similar to the purpose of Masuda (2015), except that the scale of the anomaly remaining in the transit data used by Masuda (2015) after removal of his regular eclipse model is about double that of Fig 2 (0.00001).

Our results, presented in Table 4 and shown in Fig 7, show that it is possible, with a judicious choice of location for the rotation axis, to largely remove the depression that appears in Fig 2 when interpreted as a gravity effect. Moreover, the change of γ_1 to that of Table 4 can reproduce the the Rossiter effect with essentially the same χ^2 quality of fit as that of Table 3, the obliquity moving to the same 110° as in Table 4 by the optimisation process. Note, though, that the rotation velocity is still $\sim 50\%$ up on the (uppermost) value of that of Lund et al. (2014), while precession angle ψ is, in any case, small but positive, so not consistent with the pole position from the Rossiter effect corresponding to the (2009) spectroscopic data, which requires $\psi < 0$.

3.5 Full light-curve fitting and final parameters

The full perturbation of the light from an idealised spheroidal model can be regarded as made up of 3 terms (Budding et al., 2018; see also Shporer et al., 2011; Faigler et al., 2013; and other historic papers on close binary light curves) arising from the tidal distortion (dependent on the mass-ratio q and gravity-effect

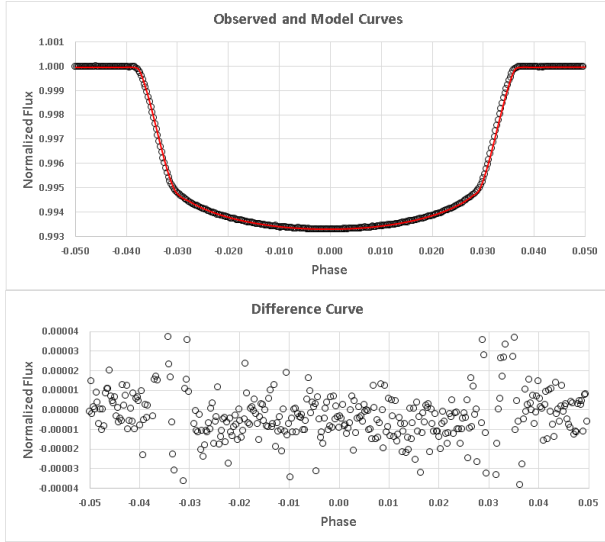


Fig. 7 Fitting to the transit region of the *Kepler-2* light curve, using data collected and binned from the full NEA compilation, with a concentration on the annular region. Relocation of the rotation axis towards the centre-right of the visible disk can remove the depression visible in Fig 2 on the basis that it is a consequence of gravity-heating of the surface over which the planet passes. The partial phases, for which the limb-darkening errors become relatively large, are ignored for this context (see Section 3.1).

τ_1), reflection effect from the companion object (coefficient E_2) and the Doppler effect from the star’s orbital motion (K_1); thus, essentially:

$$\Delta L = \Delta L_{q,\tau_1} + \Delta L_{E_2} + \Delta L_{K_1} . \quad (4)$$

Formula (4) is strictly valid only through the un-eclipsed phases. During eclipses the ΔL s are replaced by expressions of the form $(\Delta - \delta)L$, where δ indicates that some proportion of the light perturbation Δ is eclipsed out. In practice, the $\Delta L_{q,\tau_1}$ term is very small in the planetary transit phases; and so is ΔL_{E_2} , although, clearly with a visible occultation, the planet’s light loss is that of its reflected light. The Doppler term becomes noticeable in the transit if the star’s rotation is sufficiently high, leading to a photometric parallel with the spectroscopic Rossiter effect discussed in the previous subsection. This can be shown to be of order $\alpha V_{\text{rot}} \sin i_* k^2 / c$ (Shporer et al., 2012), where α is a wavelength and temperature related coefficient of order unity, similar to that affecting τ in Section 3.1. The velocity ratio is already of order 10^{-5} ; when we multiply by the other small factors the contribution becomes insignificant in the present case.

The coefficients of these three terms in the out-of-eclipse regions might be regarded as adjustable parameters (e.g. Lillo-Box et al., 2014). In practice, the scale

Table 5 Curve fitting results for the complete set of *Kepler-2* photometry over the whole range of phases.

Parameter	Value	Error
U	1.0000194	5×10^{-7}
$\Delta\phi_0$ (deg)	0.014	0.009
q	0.00101	0.00042
τ_1	0.87	0.01
E_2	0.202	0.003
Δl	0.000009	—
χ^2/ν	1.12	—

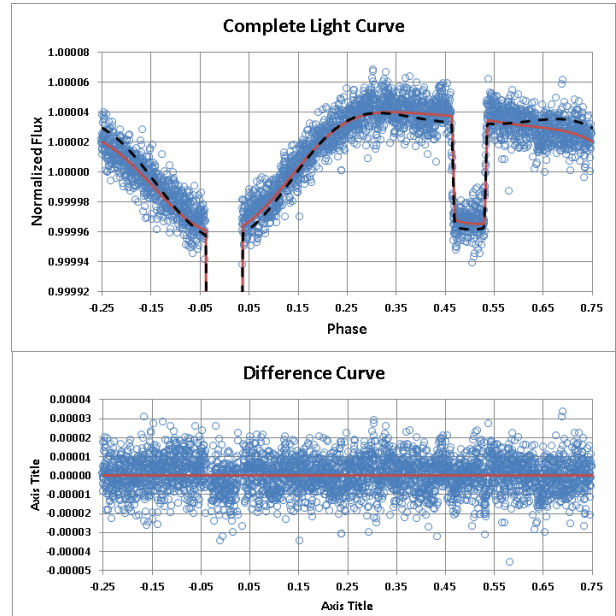


Fig. 8 The complete light curve is shown with corresponding residuals (lower panel). The optimal model’s direct tidal, reflection and Doppler effects can be seen (dashed). The better-fitting curve (continuous) comes from a slight ‘cleaning’ of the model (Section 4 of text).

of the minute $\sim 10^{-6}$ orbital Doppler effect should be specified by the prior mass M_* and the already confirmed mass ratio q and orbital inclination i that cannot be too far from 90° for eclipses to occur. Allowing ΔL_{K_1} to become a separate free parameter raises physical inconsistency as well as possible mathematical determinacy issues (Barclay et al., 2015). In our findings, however, the apparent Doppler effect in the light curve appears significantly greater than its theoretically predicted value. This point was already noticed by Esteves et al. (2013) and Faigler & Mazeh (2015).

Our results of fitting the full light curve are given in Table 5, where optimal fittings to the binned data concerned the mean reference flux U , the mass-ratio q and its closely correlated gravity-parameter τ_1 , together with the reflection coefficient E_2 ; the other parameters

Table 6 Curve fitting the complete set of Kepler-2 photometry over the whole range of phases: empirical adjustment of the leading terms.

Coefficient	Value (ppm)	Error
a_0	0.1	0.5
a_1	0.0	0.7
b_1	4.2	0.7
a_2	4.4	0.7
b_2	-0.8	0.7
Δl	0.9	—
χ^2/ν	0.93	—

having been fixed from previous fittings. We can regard E_2 as proportional to the geometric albedo A_g for the limiting case of a full radiator obeying Lambert’s law (Budding et al., 2018). Allowing E_2 to depart from this ideal case as a scaling factor for the returned light involves the same kind of interpretation as having an empirical A_g that differs from the Bond albedo in dependence on the surface properties. Thus a high E_2 value is suggestive of clouds or efficient light-scattering atmospheric particles. In fact, optimal values from curve-fitting experiments remained close to the luminous efficiency formula of Hosokawa (1958), for which $E_2 \approx 0.25$. This is an order of magnitude higher than the corresponding coefficient for *Kepler-1* (Budding et al., 2018).

The fitting for the complete light curve has a comparable overall quality of fit (χ^2/ν) to that of the transit region of Table 4 with the adopted datum error of 9 ppm, but that is still somewhat higher than the 7 ppm that could be expected from the raw measurements if the residuals were due only to Poissonian photon noise (Section 3.1). The derived mass ratio is slightly less than that from Winn et al. (2009). The finally adopted light curve model and residuals are shown in Fig 8.

There is a small difference between the best-fitting unaligned asynchronous WINFITTER model (dashed curve) and a fitting corresponding to an empirically ‘cleaned’ model (continuous curve). In this the residuals from the original light curve were fitted with a low-order Fourier decomposition consisting of only the constant, phase and $2\times$ phase terms, i.e.

$$\Delta L_{\text{res}} = a_0 + a_1 \cos \phi + b_1 \sin \phi + a_2 \cos 2\phi + b_2 \sin 2\phi. \quad (5)$$

The procedure resembles that of Zeilik et al. (1988) in the context of distorted close binary system light curves. The results are presented in Table 6.

Given the very low scale and separability of the Fourier terms we may regard b_1 as the above-mentioned increase on the ΔL_{K_1} contribution and a_2 as a slight

Table 7 Reference parameters: derived and literature comparisons. Conversion factors were calculated using values from Allen (1973), such as for the solar radius.

Parameter	Value	Error	Lit.
$M_\star \odot$	1.53	0.09	1.53
$M_p \text{ Jup}$	1.80	0.13	1.67
$a \text{ km} \times 10^6$	5.72	0.19	5.50
$R_\star \text{ km} \times 10^6$	1.46	0.08	1.36
$R_p \text{ km} \times 10^5$	1.15	0.07	1.03
$\rho_\star \text{ SI} \times 10^{-3}$	0.24	0.04	0.29
$\rho_p \text{ SI} \times 10^{-3}$	0.48	0.06	0.56
A_g	0.25	0.02	0.27

decrease on the tidal term. These points are considered below.

4 Summary and discussion

Table 7 lists our adopted set of absolute parameters, calculated from taking into account the results of the analyses in Tables 1 to 5, together with corresponding error estimates. The numbers in Table 7, that depend on separately determined and often less accurately known priors, are shown with the corresponding parameters from the NEA archive, supplemented with other literature data mentioned in Section 2.2. The two sets of results are reasonably compatible when compared with the error estimates, though our findings are for somewhat larger, less condensed, bodies.

Previous discussions of the ellipticity $\Delta L_{q,\tau_1}$ tend to be limited to the principle ($-\cos 2\phi$) term and taken to be independent of the reflection ($\sim \cos \phi$) and Doppler ($\sin \phi$) effects. We could therefore expect our more detailed formulation to give a more accurate result. But this possibility of high accuracy materializes only if there are no other factors in the data than those allowed for in the model. Fig 8 (upper panel) shows that this is not quite the case.

In fact, by adding the low-order Fourier components of Table 6 into the fitting function, the $\sin \phi$ term increases its amplitude to ~ 5 ppm. But this is ~ 6 times the scale of the Doppler-effect amplitude that can be accurately specified from the K_1 value of Table 3. The conclusion must then be that there are other contributing factors to the light-curve not included in the model. This seems self-evident for the asymmetric term in $\sin \phi$.

Fig 8 shows that the increase in the $\sin \phi$ term in the first half of the light curve closely matches the decrease in the leading ellipticity term there; whereas in

the second half of the curve the two decreases support each other, making the net asymmetry of the light curve significantly greater than in the standard model. The tidal and reflection terms are to some extent correlated, since there is also a tidal term in $\cos \phi$. However, from Table 6 we deduce that any such residual effects are not so significant against the scale of measurement error.

The sense of the persisting asymmetry in Fig 8 is different from that of *Kepler-1*, where it is very small but in reasonable agreement with the model, and *Kepler-13*, where the rise in the second half of the light cycle overcompensates for the Doppler effect and brings the two observed maxima to almost the same level. This latter situation agrees with the clouding scenario of von Paris et al. (2016), in which the ‘morning’ (western, approaching) limb is brightened when westerly winds spill over beyond the night-time terminator, producing increased cloud and brightening the approaching planet. For *Kepler-2* the prevailing tendency seems to be in the opposite direction, according to Fig 8, conforming more with the eastward hot-spot shift model of Faigler & Mazeh (2015), in which the afternoon (eastern, receding) limb becomes relatively bright. The difference between these otherwise generally comparable hot jupiters on this matter lends support to the fluctuating surface-weather discussion of Armstrong et al. (2016).

In Fig 8 we see that the light level at the centre of the planetary occultation is closely similar to that just outside the transit eclipse, tending to reinforce the scenario referred to by Borucki et al. (2009) and Wong et al. (2016) of limited heat transfer between the illuminated and non-illuminated hemispheres of the planet. But the irregularity in the light curve residuals around the primary minimum region, of order a few ppm, suggest that the Lambertian reflection model may not be adequate to cover the physics of the situation. The model adopts that the inherent light of the planet is zero, but the anomaly about the transit suggests the possibility of a low backwarming effect from the heated surface of the planet.

The planet has a Safronov parameter ($\Theta = q/r_2 = 0.049 \pm 0.008$; Safronov, 1972) and therefore within the ‘Class I’ grouping of the more massive hot jupiters. Hansen & Barman (2007) suggested that Θ should be connected to the equilibrium temperature of a planet in view of atmospheric evaporation tending to decrease q and increase r_2 . This inference may be connected to the moving bright spots or strong winds discussed by Borucki et al. (2009), Esteves et al. (2015), Armstrong et al. (2016) and others. Stability of the outer regions of hot jupiters continues to stimulate lively discussion (Christian & Lund, 2010; Madhusudhan et al., 2018).

In Section 3 we noted that there was a disparity in the location of the polar axis between the spectroscopic and photometric analyses. There are several lines of thought that bear on this. Firstly, although the pole is located in different quadrants of the disk at phase zero in these different findings, there is a general agreement (also with Winn et al., 2009), that the rotation axis is not far from the line of sight (see also, Southworth, 2017). Our spectroscopic analysis referred to the relatively high degree of scatter in the transit-phase data, though the separation of the two pole positions is greater than reasonable error estimates would allow their coincidence. Adopting, then, that these two analyses do result in essentially different axis positions, there arise such explanation possibilities as (a) the spectroscopic or photometric modelling retains some inadequacy, or (b) there has been a measurable movement of the pole between mid-2008 (the Subaru observations) and mid-2011 (middle of the Kepler series).

Concerning point(a) and in relation to the spectroscopic results, it can be kept in mind that the conventional model adopted is that the effect of a transiting planet on a spectral line’s Doppler shift arises from a convolution with other processes, particularly instrumental broadening. The measured movement of the line is then that of its ‘light centre’ (Hirano et al., 2011; Brown et al., 2017). If, with a very high resolution system, a line profile broadened only by rotation were to be recorded there would be no Rossiter effect on the centre of the line. The eclipsing planet would simply register as a feature on the profile.¹⁰ The HDS data shown in Fig 7 is from a high resolution spectrograph, but it is not clear to what extent this may bear on the data-processing used to determine reported wavelength shifts.

Similarly, with regard to the photometry, stars may be affected by other local darkening or brightening mechanisms than the gravity effect. Even within the physics of that effect there is scope for departure from the WINFITTER specification of rigid body rotation, for example, which stars do not strictly conform to. At the same time, stellar circulation currents may counter the classic von Zeipel formulation of this effect (Kirbyyık & Smith, 1976). Also, the mid-F type classification of the host star suggests the possibility of a ‘polar spot’ (Schrijver & Title, 2001; Berdyugina, 2002; Oshagh et al., 2015). Instead of the depression in Fig 2 being due to the eclipse of a bright region, it could be that the raised part of the residuals distribution in the minimum is due to the eclipse of a somewhat cooler part of

¹⁰This is the basis of the ‘Doppler imaging’ technique (cf. Vogt, 1983).

the surface. Other modelling or data inadequacies were mentioned in Section 2.2. Having said this, the fairly low extent of model inadequacy relative to data scatter can be judged by the difference between the continuous and dashed lines in Fig 8.

Point (b) requires a movement of several deg in ~ 3 y, i.e. a precession period of order a few hundred y only. This is about an order of magnitude less than could be reasonably expected for the configuration (see, for example, the calculation for the comparable case of *Kepler-13* in Budding et al., 2018). It seems, then, much more likely that the apparent shifts of axis position between the 2008 and 2011 (averaged) data-sets are related to inadequacy of modelling for the spectroscopic Rossiter effect, or additional, unprogrammed, surface inhomogeneities of brightness affecting the photometric analysis, than real short-term movements of the star's rotation axis. Continued detailed monitoring of *Kepler-2* (HAT-P-7A) are required to help solve these remaining problems of the system.

5 Acknowledgements

It is a pleasure to thank Prof. Osman Demircan and the colleagues in the Physics Department of COMU (Çanakkale, Turkey) for their interest and support of this programme. The research has been supported by TÜBİTAK (Scientific and Technological Research Council of Turkey) under Grant No. 113F353. Additional help and encouragement for this work has come from the National University of Singapore, particularly through Prof. Lim Tiong Wee of the Department of Statistics and Applied Probability. This research has made use of the NASA Exoplanet Archive, which is operated by the California Institute of Technology, under contract with the National Aeronautics and Space Administration under the Exoplanet Exploration Program. This work has made use of data from the European Space Agency (ESA) mission *Gaia* (<https://www.cosmos.esa.int/gaia>), processed by the *Gaia* Data Processing and Analysis Consortium (DPAC, <https://www.cosmos.esa.int/web/gaia/dpac/consortium>). TB & EB wish to record our gratitude to the late Prof. Denis J. Sullivan (Victoria University of Wellington, NZ) for his support of this and related programmes, and extend our condolences to his family.

References

- Albrecht, S., Winn, J. N., Johnson, J. A., Howard, A. W., Marcy, G. W., Butler, R. P., Arriagada, P., Crane, J. D., Shectman, S. A., Thompson, I. B., Hirano, T., Bakos, G., & Hartman, J. D., 2012, *ApJ*, 757, 18
- Allen, C.W., 1973, *Astrophysical Quantities*, Athlone Press, University of London
- Alonso, R., Brown, T. M., Torres, G., Latham, D. W., Sozzetti, A., Mandushev, G., Belmonte, J. A., Charbonneau, D., Deeg, H. J., Dunham, E. W., O'Donovan, F. T. & Stefanik, R. P., 2004, *ApJ*, 613, L153
- Angerhausen, D., DeLarme, E., & Morse, J. A., 2015, *PASP*, 127, 1113
- Armstrong, D. J., de Mooij, E., Barstow, J., Osborn, H. P., Blake, J., & Sanjeev, N. F., 2016, *Nature Astronomy*, 1, 0004
- Banks, T.S., & Budding, E., 1990, *ApSS*, 167, 221
- Barclay, T., Endl, M., Huber, D., Foreman-Mackey, D., Cochran, W. D., MacQueen, P. J., Rowe, J. F., & Quintana, E. V., 2015, *ApJ*, 800, 46
- Barnes, J. W., Linscott, E. & Shporer, A., 2011, *ApJS*, 197, 10
- Batalha, N. M., Rowe, J. F., Bryson, S. T., Barclay, T., Burke, C. J., Caldwell, D. A., Christiansen, J. L., Mullally, F., Thompson, S. E., Brown, T. M., Dupree, A. K., Fabrycky, D. C., Ford, E. B., Fortney, J. J., Gilliland, R. L., Isaacson, H., Latham, D. W., Marcy, G. W., Quinn, S. N., Ragozzine, D., Shporer, A., Borucki, W. J., Ciardi, D. R., Gautier, III, T. N., Haas, M. R., Jenkins, J. M., Koch, D. G., Lissauer, J. J., Rapin, W., Basri, G. S., Boss, A. P., Buchhave, L. A., Carter, J. A., Charbonneau, D., Christensen-Dalsgaard, J., Clarke, B. D., Cochran, W. D., Demory, B.-O., Desert, J.-M., Devore, E., Doyle, L. R., Esquerdo, G. A., Everett, M., Fressin, F., Geary, J. C., Girouard, F. R., Gould, A., Hall, J. R., Holman, M. J., Howard, A. W., Howell, S. B., Ibrahim, K. A., Kinemuchi, K., Kjeldsen, H., Klaus, T. C., Li, J., Lucas, P. W., Meibom, S., Morris, R. L., Prša, A., Quintana, E., Sanderfer, D. T., Sasselov, D., Seader, S. E., Smith, J. C., Steffen, J. H., Still, M., Stumpe, M. C., Tarter, J. C., Tenenbaum, P., Torres, G., Twicken, J. D., Uddin, K., Van Cleve, J., Walkowicz, L. & Welsh, W. F., 2013, *ApJS*, 204, 24
- Benomar, O., Masuda, K., Shibahashi, H., & Suto, Y., 2014, *PASJ*, 66, 94
- Berdugina, S. V., 2002, *AN*, 323, 192-195
- Bevington, P.R., 1969, *Data Reduction and Error Analysis for the Physical Sciences*, McGraw-Hill, New York
- Borucki, W. J., Koch, D. G., Basri, G. B., Caldwell, D. A., Caldwell, J. F., Cochran, W. D., Devore, E., Dunham, E. W., Geary, J. C., Gilliland, R. L., Gould, A., Jenkins, J. M., Kondo, Y., Latham, D. W. & Lissauer, J. J., 2003, in *Scientific Frontiers in Research on Extrasolar Planets*, Eds. D. Deming & S. Seager, ASP Conf. Ser. 294, 427
- Borucki, W. J., Koch, D., Jenkins, J., Sasselov, D., Gilliland, R., Batalha, N., Latham, D. W., Caldwell, D., Basri, G., Brown, T., Christensen-Dalsgaard, J., Cochran, W. D., DeVore, E., Dunham, E., Dupree, A. K., Gautier, T., Geary, J., Gould, A., Howell, S., Kjeldsen, H., Lissauer, J., Marcy, G., Meibom, S., Morrison, C., Borucki, W. J., Koch, D. G., Basri, G., Batalha, N., Brown, T. M., Bryson, S. T., Caldwell, D., Christensen-Dalsgaard, J., Cochran, W. D., DeVore, E., Dunham, E., Gilliland, R., Gould, A., Howell, S. B., Jenkins, J. M., Latham, D. W., Lissauer, J. J., Marcy, G. W., Rowe, J., Sasselov, D., Boss, A., Charbonneau, D., Ciardi, D., Doyle, L., Dupree, A. K., Ford, E. B., Fortney, J., Holman, M. J., Seager, S., Steffen, J. H., Tarter, J., Welsh, W. F., Allen, C., Buchhave, L. A., Christiansen, J. L., Clarke, B. D., Das, S., Desert, J.-M., Endl, M., Fabrycky, D., Fressin, F., Haas, M., Horsch, E., Howard, A., Isaacson, H., Kjeldsen, H., Kolodziejczak, J., Kulesa, C., Li, J., Lucas, P. W., Machalek, P., McCarthy, D., MacQueen, P., Meibom, S., Miquel, T., Prsa, A., Quinn, S. N., Quintana, E. V., Ragozzine, D., Sherry, W., Shporer, A., Tenenbaum, P., Torres, G., Twicken, J. D., Van Cleve, J., Walkowicz, L., Witteborn, F. C., & Still, M., 2011, *ApJ*, 736, 19
- Boué, G., Montalto, M., Boisse, I., Oshagh, M., & Santos, N. C., 2013, *A&A*, 550, A53
- Brown, T. M., Latham, D. W., Everett, M. E., & Esquerdo, G. A., 2011, *AJ*, 142, 112
- Brown, D. J. A., Triaud, A. H. M. J., Doyle, A. P., Gillon, M., Lendl, M., Anderson, D. R., Collier Cameron, A., Hébrard, G., Hellier, C., Lovis, C., Maxted, P. F. L., Pepe, F., Pollacco, D., Queloz, D., & Smalley, B., 2017, *MNRAS*, 464, 810-839
- Budding, E., 1974, *ApSS*, 22, 87
- Budding, E. & Demircan, O., 2007, *Introduction to Astronomical Photometry*, CUP
- Budding, E., Rhodes, M. D., Püsküllü, Ç., Ji, Y., Erdem, A., & Banks, T., 2016, *Ap&SS*, 361, 346
- Budding, E., Püsküllü, Ç. & Rhodes, M.D., 2018, *Ap&SS*, 363, 60
- Butler, R. P., Marcy, G. W., Williams, E., McCarthy, C., Dosanji, P., & Vogt, S. S., 1996, *PASP*, 108, 500
- Butler, R. P., Wright, J. T., Marcy, G. W., Fischer, D. A., Vogt, S. S., Tinney, C. G., Jones, H. R. A., Carter, B. D., Johnson, J. A., McCarthy, C., & Penny, A. J., 2006, *ApJ*, 646, 505-522
- Catling, D.C. & Kasting, J.F., 2017, *Atmospheric Evolution on Inhabited and Lifeless Worlds*
- Christensen-Dalsgaard, J., Kjeldsen, H., Brown, T. M., Gilliland, R. L., Arentoft, T., Frandsen, S., Quirion, P.-O., Borucki, W. J., Koch, D., & Jenkins, J. M., 2010, *ApJL*, 2010, 713, L164-L168
- Christian, D.J. & Lund, M.B., 2010, *AAS-DPS*, 42, 27
- Daemgen, S., Hormuth, F., Brandner, W., Bergfors, C., Janson, M., Hippler, S., & Henning, T., 2009, *A&A* 498, 567
- Dotson, J., 2019, <https://keplerscience.arc.nasa.gov>
- Dvoskry, G., 2016, <https://gizmodo.com/clouds-of-rubies-and-sapphires-glow-on-this-distant-exo-1790044935>, retrieved 06-Feb-2020.
- Esteves, L. J., De Mooij, E. J. W. & Jayawardhana, R., 2013, *ApJ*, 772, 51
- Esteves, L. J., De Mooij, E. J. W. & Jayawardhana, R., 2015, *ApJ*, 804, 150
- Faedi, F., Staley, T., Gómez Maqueo Chew, Y., Pollacco, D., Dhital, S., Barros, S. C. C., Skillen, I., Hebb, L., Mackay, C., & Watson, C. A., 2013, *MNRAS*, 433, 2097-2106

- Faigler, S., Tal-Or, L., Mazeh, T., Latham, D. W., & Buchhave, L. A., 2013, *ApJ*, 771, 26
- Faigler, S. & Mazeh, T., 2015, *ApJ*, 800, 73
- Gaia Collaboration, 2018, *A&A*, 616, A1
- Guzik, J. A.; Chaplin, W. J.; Handler, G. & Pigulski, A. (Eds.), 2014, *Precision Asteroseismology*, 301
- Hansen, B.M.S. & Barman, T., 2007, *ApJ*, 671, 861
- Hirano, T., Suto, Y., Winn, J. N., Taruya, A., Narita, N., Albrecht, S., & Sato, B., 2011, *ApJ*, 742, 69
- Hosokawa, Y., 1958, *PASJ* 10, 120
- Howard, A. (and SIM Team), 2009, *BAAS*, 214, 750
- Johnson, M. C., Cochran, W. D., Albrecht, S., Dodson-Robinson, S. E., Winn, J. N., & Gullikson, K., 2014, *ApJ*, 790, 30
- Kipping, D.M. & Spiegel, D.S., 2011, *MNRAS*, 417, 88
- Kirbyrik, H. & Smith, R. C., 1976, *MNRAS*, 176, 103-129
- Kopal, Z., 1959, *Close Binary Systems*, Chapman & Hall, London & New York
- Kourganoff, V., 1952, *Basic methods in transfer problems; radiative equilibrium and neutron diffusion*, Oxford, Clarendon Press
- Libralato, M., Nardiello, D., Bedin, L. R., Borsato, L., Granata, V., Malavolta, L., Piotto, G., Ochner, P., Cunial, A., & Nascimbeni, V., 2016, *MNRAS*, 463, 1780-1796
- Lillo-Box, J., Barrado, D., Henning, Th., Mancini, L., Cicceri, S., Figueira, P., Santos, N. C., Aceituno, J., & Sánchez, S. F., 2014, *A&A*, 568, L1
- Lillo-Box, J., Ribas, A., Barrado, D., Merín, B., & Bouy, H., 2016, *A&A*, 592, A32
- Lund, M. N., Lundkvist, M., Silva Aguirre, V., Houdek, G., Casagrande, L., Van Eylen, V., Campante, T. L., Karoff, C., Kjeldsen, H., Albrecht, S., Chaplin, W. J., Nielsen, M. B., Degroote, P., Davies, G. R., & Handberg, R., 2014, *A&A*, 570, A54
- Madhusudhan, N., Bitsch, B., Johansen, A., & Eriksson, L., 2017, *MNRAS*, 469, 4102-4115
- Masuda, K., 2015, *ApJ*, 805, 28
- Mazeh, T., Nachmani, G., Sokol, G., Faigler, S., & Zucker, S., 2012, *A&A*, 541, A56
- McLaughlin, D. B., 1924, *ApJ*, 60, 22
- McNally, D., 1965, *Obs*, 85, 166-169
- Mislis, D. & Hodgkin, S., 2012, *MNRAS*, 422, 1512-1517
- Morris, C. K., Barclay, J. R., Anderson, T. R., & Walter, M. T., 2013, *AGU Fall Meeting Abstracts*, H13E-1389
- Narita, N., Sato, B., Hirano, T., & Tamura, M., 2009, *PASJ*, 61, L35-L40
- Neuhäuser, R., Errmann, R., Berndt, A., Maciejewski, G., Takahashi, H., Chen, W. P., Dimitrov, D. P., Pribulla, T., Nikogossian, E. H., Jensen, E. L. N., Marschall, L., Wu, Z.-Y., Kellerer, A., Walter, F. M., Briceño, C., Chini, R., Fernandez, M., Raetz, S., Torres, G., Latham, D. W., Quinn, S. N., Niedzielski, A., Bukowiecki, L., Nowak, G., Tomov, T., Tachihara, K., Hu, S. C.-L., Hung, L. W., Kjurkchieva, D. P., Radeva, V. S., Mihov, B. M., Slavcheva-Mihova, L., Bozhinova, I. N., Budaj, J., Vaňko, M., Kundra, E., Hambálek, L., Krushevska, V., Movsesian, T., Harutyunyan, H., Downes, J. J., Hernandez, J., Hoffmeister, V. H., Cohen, D. H., Abel, I., Ahmad, R., Chapman, S., Eckert, S., Goodman, J., Guerard, A., Kim, H. M., Koontharana, A., Sokol, J., Trinh, J., Wang, Y., Zhou, X., Redmer, R., Kramm, U., Nettelmann, N., Mu-grauer, M., Schmidt, J., Moualla, M., Ginski, C., Marka, C., Adam, C., Seeliger, M., Baar, S., Roell, T., Schmidt, T. O. B., Trepl, L., Eisenbeiß, T., Fiedler, S., Tetzlaff, N., Schmidt, E., Hohle, M. M., Kitze, M., Chakrova, N., Gräfe, C., Schreyer, K., Hambaryan, V. V., Broeg, C. H., Koppenhoefer, J., & Pandey, A. K., 2011, *AN*, 332, 547
- Nielsen, M. B., Gizon, L., Schunker, H., & Karoff, C., 2013, *Progress in Physics of the Sun and Stars: A New Era in Helio- and Asteroseismology*, 479, 137
- O'Donovan, F. T., Charbonneau, D., Mandushev, G., Dunham, E. W., Latham, D. W., Torres, G., Sozzetti, A., Brown, T. M., Trauger, J. T., Belmonte, J. A., Rabus, M., Almenara, J. M., Alonso, R., Deeg, H. J., Esquerdo, G. A., Falco, E. E., Hillenbrand, L. A., Roussanova, A., Stefanik, R. P., & Winn, J. N., 2006, *ApJ*, 651, L61
- Oshagh, M., Santos, N. C., Figueira, P., Adibekyan, V. Zh., Santerne, A., Barros, S. C. C., & Lima, J. J. G., 2015, *A&A*, 583, L1
- Pál, A., Bakos, G. Á., Torres, G., Noyes, R. W., Latham, D. W., Kovács, G., Marcy, G. W., Fischer, D. A., Butler, R. P., Sasselov, D. D., Sipőcz, B., Esquerdo, G. A., Kovács, G., Stefanik, R., Lázár, J., Papp, I., & Sári, P., 2008, *ApJ*, 680, 1450-1456
- Rhodes, M.D. & Budding, E., 2014, *Ap&SS*, 351, 451-471
- Rhodes, M.D., 2019, *WinFitter v.6.4 User Manual*
- Rossiter, R.A., 1924, *ApJ* 60, 15
- Rowe, J., Bryson, S. T., Caldwell, D. A., Christiansen, J. L., Haas, M. R., Jenkins, J. M., Machalek, P., Mullally, F. R., Still, M., & Thompson, S. E., 2011, *AAS Meeting Abstracts* 218, 43, 211
- Safronov, V.S., 1972, *IAUSymp.* 45, Reidel, Dordrecht, p 329
- Santerne, A., Moutou, C., Barros, S. C. C., Damiani, C., Díaz, R. F., Almenara, J. -M., Bonomo, A. S., Bouchy, F., Deleuil, M., Hébrard, G., 2012, *A&A*, 544, L12
- Schlesinger, F., 1910, *Publications of the Allegheny Observatory of the University of Pittsburgh*, 1, 123
- Schrijver, C. J. & Title, A. M., 2001, *ApJ*, 551, 1099-1106
- Shporer, A., Jenkins, J. M., Rowe, J. F., Sanderfer, D. T., Seader, S. E., Smith, J. C., Still, M. D., Thompson, S. E., Twicken, J. D., & Welsh, W. F., 2011, *AJ*, 142, 195
- Shporer, A., Brown, T., Mazeh, T., & Zucker, S., 2012, *NewA*, 17, 309-315
- Shibahashi, H. & Lynas-Gray, A. E. (Eds.), 2013, *Progress in Physics of the Sun and Stars: A New Era in Helio- and Asteroseismology*, 479
- Smith, J. C., Stumpe, M. C., Van Cleve, J. E., Jenkins, J. M., Barclay, T. S., Fanelli, M. N., Girouard, F. R., Kolodziejczak, J. J., McCauliff, S. D., Morris, R. L., & Twicken, J. D., 2012, *PASP*, 124, 1000
- Southworth, J., 2017, *PASP*, 129(2), 24401
- Sozzetti, A., Torres, G., Charbonneau, D., Latham, D. W., Holman, M. J., Winn, J. N., Laird, J. B., & O'Donovan, F. T., 2007, *ApJ*, 664, 1190
- Stumpe, M. C., Smith, J. C., Van Cleve, J. E., Twicken, J. D., Barclay, T. S., Fanelli, M. N., Girouard, F. R., Jenkins, J. M., Kolodziejczak, J. J., McCauliff, S. D., & Morris, R. L., 2012, *PASP*, 124, 985
- Twicken, J. D., Chandrasekaran, H., Jenkins, J. M., Gunter, J. P., Girouard, F., & Klaus, T. C., 2010, *SPIE Conf. Ser.* 7740, p77401-U-1

- Van Eylen, V., Lindholm Nielsen, M., Hinrup, B., Tingley, B., & Kjeldsen, H., 2013, *ApJL*, 774, L19
- von Paris, P., Gratier, P., Bordé, P., Leconte, J., & Selsis, F., 2016, *A&A*, 589, A52
- Welsh, W. F., Seager, S., Fortney, J. J., Rowe, J. F., Orosz, J. A., Borucki, W. J., & Koch, D., 2010, *American Astronomical Society Meeting Abstracts* 215, 42, 318
- Winn, J. N., Johnson, J. A., Albrecht, S., Howard, A. W., Marcy, G. W., Crossfield, I. J., & Holman, M. J., 2009, *ApJL*, 703, L99-L103
- Wong, I., Knutson, H. A., Kataria, T., Lewis, N. K., Burrows, A., Fortney, J. J., Schwartz, J., Shporer, A., Agol, E., Cowan, N. B., Deming, D., Désert, J.-M., Fulton, B. J., Howard, A. W., Langton, J., Laughlin, G., Showman, A. P., & Todorov, K., 2016, *ApJ*, 823, 122
- Zeilik, M., de Blasi, C., Rhodes, M., & Budding, E., 1988, *ApJ*, 332, 293-298